Towards wireless highly sensitive capacitive strain sensors based on gold colloidal nanoparticles

Hussein Nesser, Jérémie Grisolia, Thomas Alnasser, Benoit Viallet, Laurence Ressier

Towards wireless highly sensitive capacitive strain sensors based on gold colloidal nanoparticles†

H. Nesser, J. Grisolia, * T. Alnasser, B. Viallet and L. Ressier

We designed, produced and characterized new capacitive strain sensors based on colloidal gold nanoparticles. The active area of these sensors, made up of a 1 mm^2 close-packed assembly of gold nanoparticles between interdigitated electrodes, was designed to achieve measurable capacitance (>~1 pF) and overcome parasitic capacitances. Electro-mechanical experiments revealed that the sensitivity of such capacitive sensors increases in relation to the size of the nanoparticles. In the case of 14 nm gold NPs, such sensors present a relative capacitance variation of −5.2% for a strain of 1.5%, which is more than 5 times higher than that observed for conventional capacitive strain gauges. The existence of two domains (pure capacitive domain and mixed capacitive–resistance domain) as a function of the frequency measurement allows for the adaptation of sensitivity of these capacitive sensors. A simple low-cost circuit based on a microcontroller board was finally developed to detect the capacitance variations of such NP based strain sensors. This low-cost equipment paves the way for the development of an entirely wireless application set-up.

I Introduction

In many fields, the deployment of sensors is limited by wired connections, resulting in excess weight, high electrical consumption and the generation of installation problems. Hence, wireless sensor networks (WSNs) are currently being developed and have already a large number of applications for both safety-critical and non-safety critical distributed systems.[1] As an example, potential benefits for aircraft systems would include weight reduction, ease of maintenance and increased monitoring capability. In the context of such a wireless application, the resistive strain gauges commonly used for strain measurements have disadvantages because they are limited by wires, read out with low impedance and consequently result in high power consumption. By contrast, capacitive strain gauges are very promising for the development of WSNs, because such sensors can be implemented in oscillating circuits whose emitted frequency would correspond to their capacitance variations. Moreover, they can have lower power consumption by working with AC measurements.

Several conceptions of capacitive strain sensors have recently been presented in the literature, including parallel-plate capacitors,[2,3] interdigitated electrodes,[4–7] or even rosette-type resistive electrode arrays.[8] Other types of strain gauges are based on elastic polymers deposited in different layers.[2,3,6–8] Notably, strain sensors based on flexible PDMS filled with nanoparticles (NPs) are well adapted to a large number of versatile applications in a variety of fields ranging from interactive electronics,[9] biomedicine and device implants,[10] to robotics[11] and aeronautics. However, all these capacitive strain sensors unfortunately have very low sensitivities as assessed by a gauge factor GF_C around 1 (ref. 12) to 1.45.[13]

One solution for increasing the sensitivity of capacitive strain sensors would be to exploit the electronic properties of colloidal NPs. Indeed, assemblies of conductive colloidal nanoparticles protected by organic ligands have elicited considerable favorable attention for several sensing applications (gas sensors, temperature sensors ...).[14–17] One of the recent applications based on inter-particle electronic coupling is strain sensing measurements.[18–22] Resistive strain gauges were built from assemblies of colloidal conductive nanoparticles on flexible substrates. Briefly, the high sensitivity of these devices is due to the exponential dependence of tunnel resistance on the separation between adjacent nanoparticles in the NP assembly.[23,24] The total resistance R of the NP assemblies can be derived from the association in series and parallel of a number of tunnel junctions schematized by a parallel R–C electrical model between two metallic nanoparticles (Fig. S1 ESI†). It can then be roughly expressed as:[25–30]

$$R \propto e^{-\left[\beta l + \frac{E_C}{k_B T}\right]} \quad (1)$$

Université de Toulouse, LPCNO, INSA-CNRS-UPS, 135 avenue de Rangueil, Toulouse 31077, France. E-mail: jeremie.grisolia@insa-toulouse.fr

†Electronic supplementary information (ESI) available: Conception of the capacitive sensor, chemical synthesis of gold nanoparticles, capacitive strain gauge fabrication (lift-off method), temperature-dependent electron transport, inter-particle distance measurement method. See DOI: 10.1039/c7nr09685b

where β is the decay tunneling constant which depends essentially on the barrier height, l is the distance between nanoparticles, E_C is the charging energy, k_B the Boltzmann constant and T the temperature.

The electron transport on such NP assemblies thus represents a function of the tunneling decay and, more interestingly, of the Coulomb charging energy E_C. An electron flowing through these granular films must consequently overcome the tunnel barrier length l and also the Coulomb charging energy:

$$E_C = \frac{e^2}{2C} \quad (2)$$

linked to the total capacitance C of the NP assemblies, and where e is the elementary charge. Hence, as it will be shown below, an inter-nanoparticle distance variation will induce an overall capacitance variation of the NP assemblies and will be interesting to exploit in a sensor. In the literature, this term has been not used as a link for capacitive applications,[19] or simply neglected because of its low impact on the overall characteristics of the NP assemblies in comparison with β, the decay tunneling constant.[20,45] This is why it was probably not exploited to make capacitive strain sensors.

In this article, we propose to fabricate new capacitive strain gauges based on assemblies of colloidal gold NPs deposited between interdigitated electrodes. We design the electrode structure to increase the overall impact of the capacitance factor for obtaining highly sensitive capacitive strain gauges measurable by low-cost electronic equipments.

This work aims to demonstrate the potential of nanotechnology in developing strain sensors which are highly sensitive, low-cost, potentially low consumption, with consistent reliability, paving the way to wireless applications.

II Sensor design for optimized capacitive strain sensitivity

Our modeling is based on the measurement of the C_{ij} capacitance between two colloidal NPs embedded in a dielectric matrix of permittivity ε_r. Several models were proposed in the literature to calculate C_{ij}.[31–36] In this study, we chose the model of Quinn *et al.*[36] which expresses the junction capacitance between two NPs by the following equation:

$$C_{ij} = \pi\varepsilon_0\varepsilon_r d \ln(1 + d/l) \quad (3)$$

where l is the distance between two nanoparticles, d is the diameter of the nanoparticles, ε_0 is the permittivity of the vacuum and ε_r is the relative permittivity of organic ligands surrounding the NPs.

A quick calculation, using the gold NP diameter $d = 2r$ = 7 nm, an inter-particle distance l = 1.2 nm for dodecanethiol ligands, ε_r = 2.3 typical of self-assembled dodecanethiol shows that this capacitance is in the order of aF range which is well below any measurement system used in WSNs. Exploiting this capacitive feature constrains us to increase the number of nanoparticles on the NP assemblies in order to take advantage of their collective effects and get a measurable value. We then performed modeling of the capacitance of NP assemblies to design capacitive strain gauges that have capacitance reaching the range of easy measurement (*e.g.* ~1 pF) and capacitance variations greater than disturbances by surrounding parasitic capacitances (see the ESI†). We proposed to deposit the nanoparticles on a structure based on interdigitated electrodes with optimized dimensions (Fig. S2 ESI†): the active area of the sensors is made of a 1 mm^2 closed-packed assembly of gold nanoparticles integrated between interdigitated electrodes (width = 5 μm and interdigitated distance = 5 μm) (see Table 1 ESI†). It is worth noting that the chosen dimensions of the interdigitated electrodes are based on compensation between the optimum values obtained by simulation and the fabrication limitations (*e.g.* laser lithography resolution...). The total capacitance C of this geometry can be calculated using:

$$C = k \cdot C_{ij} \quad (4)$$

where k is the geometrical factor of the interdigited electrodes taking into account the capacitances in series and parallel (see the ESI†).

The derivative of the total capacitance leads to the relative capacitance variation as a function of strain, NP diameter and the inter-nanoparticle distance (see the ESI†):

$$\frac{\Delta C}{C} \simeq -\frac{d}{l \ln\left(1 + \frac{d}{l}\right)} . \varepsilon \quad (5)$$

where $\varepsilon = \frac{\Delta l}{l}$ is the strain applied to the sensor, d is the diameter of the particles, and C is the sensor capacitance.

This gives an analytical expression for the capacitive gauge factor GF_C of such sensors defined as the following equation below:

$$GF_C = \frac{\Delta C/C}{\varepsilon} = -\frac{d}{l \ln\left(1 + \frac{d}{l}\right)} \quad (6)$$

This modeling shows that the capacitance gauge factor of such capacitive strain sensors is a function of the NP and ligand sizes. Fig. 1a highlights that the increase of the nanoparticle size (given the inter-nanoparticle distance l = 1.2 nm) increases the variation of capacitance ranging from 3% for 7 nm up to 15% for NPs of 100 nm diameter for 1% of strain. Fig. 1b shows the evolution of the relative capacitance variation as a function of the strain for a 1 mm×1 mm sensor with NPs of 7, 12 and 14 nm diameters. With a 1 mm^2 sensor, one could obtain a gauge factor around 5, without taking into account the variation of capacitance due to the geometric variation. This sensitivity is five times greater than the one found in the literature based on the geometric capacitance variation.[6,12,37]

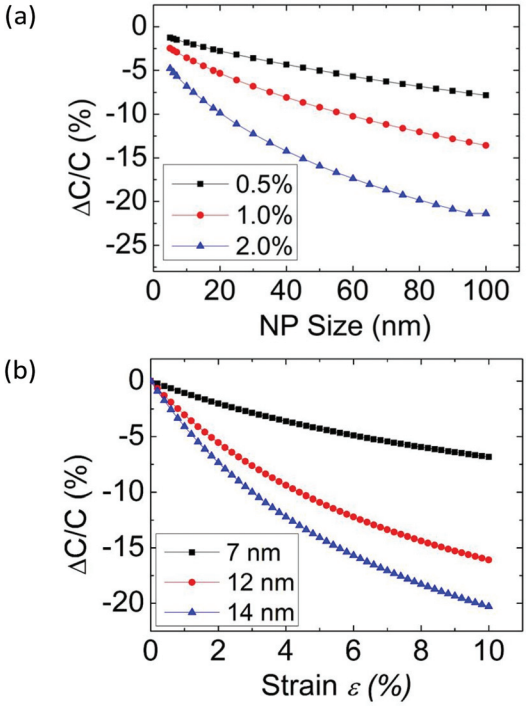

Fig. 1 (a) Theoretical influence of the NP size on the relative capacitance variation for a strain ranging from 0.5% to 2%. (b) Theoretical relative capacitance variation as a function of strain for NP size ranging from 7 nm to 14 nm.

III Fabrication of the NP-based capacitive strain sensors

The essential challenge in the fabrication of the NP-based capacitive strain sensors was to produce a uniform and defect-free close-packed assembly of gold nanoparticles over a large electrode area of 1 mm^2.

First, 7, 12 and 14 nm gold nanoparticles functionalized with dodecanethiol (C12) organic ligands were synthesized using two chemical routes. The 7 nm gold nanoparticles were synthesized following the protocol described by Zheng *et al.*[39,40] This procedure was repeated and resulted in a colloidal suspension of spherical Au NPs in toluene at a concentration of about 2×10^{15} NPs per mL as presented in the Fig. S3 ESI.† 12 and 14 nm gold nanoparticles were synthesized following the protocol described by H. Hiramatsu *et al.*[41] This procedure was further repeated and led to a colloidal dispersion of spherical gold nanoparticles in toluene at a concentration $\approx 2 \times 10^{15}$ NPs per ml as presented the Fig. S3 ESI.†

In order to increase the sensitivity of the capacitive strain sensors on the basis of the theoretical results presented in Fig. 1a, we tried to synthesize bigger gold NPs in organic solvent in the range of 20–100 nm using other chemical routes.[41,42] Unfortunately, the colloidal stability of such gold NPs requires a functionalization with long chain ligands such as polymers. This gives large internanoparticle distances, thus leading to large DC resistance exceeding 100GΩ.

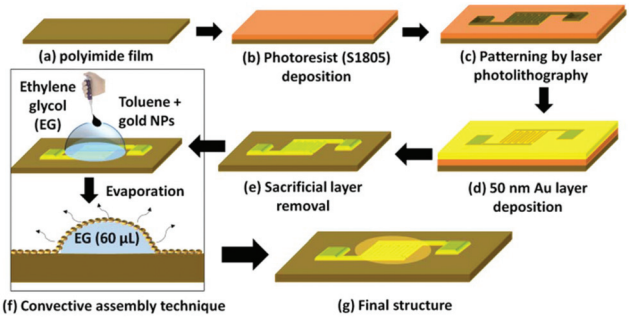

Fig. 2 Fabrication process of the capacitive NP-based strain sensors.

Secondly, interdigitated gold electrodes were fabricated on 125 µm polyimide (Upilex) films using the lift-off method (Fig. 2). A reverse pattern was created in the sacrificial stencil layer by laser photolithography (see the ESI†). Then, a 50 nm gold Au layer was deposited over the entire surface of the substrate by IBS-E ion beam sputtering. After lift-off, a 1 mm^2 sensor with 50 pairs of interdigitated electrodes 5 µm wide and 5 µm interdigitated distance was obtained and connected by external gold electrodes.

Thirdly, the gold NPs were deposited between the interdigitated electrodes by the convective assembly technique. Based on our previous work on freestanding NP monolayers over stencil substrates, we chose the liquid/liquid interface using the ethylene glycol method to assemble NP on the interdigitated electrodes.[18,46] This method involves assembling the nanoparticles at the level of the meniscus of a drop of colloidal suspension by evaporation. A 19 µL drop of a colloidal suspension of gold NPs, coated with dodecanethiol ligands, in toluene was deposited on top of a 60 µL ethylene glycol (EG) droplet located at the surface level of the substrates (Fig. 2f). EG was used instead of water to improve the long range ordering of gold NPs due to its high viscosity and low evaporation rate. In solvent evaporation at room temperature, gold NPs self-assembled as a close-packed ordered array at the surface of the EG droplet (Fig. 2f), preferably at the level of the meniscus of the drop during its evaporation.[47,48] As the EG droplet slowly evaporated over 24 h under mild heating at 55 °C, the gold NP array was transferred onto the surface of the substrate covering the entire active zone.

This assembly technique allows depositing a quite uniform and homogeneous multi-layered nanoparticle film on a large surface (1 mm^2) (Fig. 3d). At the end of the process, the thickness of the NP films not exceeding the electrode height corresponds approximately to 3 to 5 layers of NPs.

Finally, the electrical contacts can be connected by wires or by spikes on Au pad electrodes. The final sensor is shown in Fig. 3.

IV Experimental characterization

IV.1 Electro-mechanical response of capacitive strain sensors

The electrical characterization studies of capacitance were carried out with an impedance analyzer (Keysight E4990A)

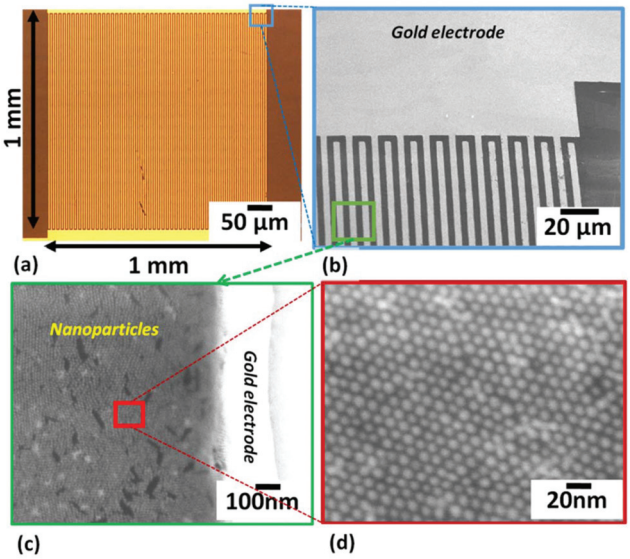

Fig. 3 (a) Optical microscopy image of the interdigitated electrode area (1 mm^2) of the sensors. (b) Zoom-in by scanning electron microscopy (SEM) of the interdigitated electrodes with a distance of 5 µm. (c, d) Successive SEM zoom-ins of the assembly of 14 nm gold nanoparticles between the electrodes.

capable of measuring the lowest capacitances in the order of fF. Measurement frequencies between f = 50 Hz and 1 MHz, for the signal produced by the E4990A Impedance Analyzer, were chosen. Capacitive strain sensors with various nanoparticle sizes (7, 12 and 14 nm) were fabricated, while a "blank" structure representing the same geometry and without nanoparticles was produced to act as a reference. An open calibration was carried out with this "blank" reference before each measurement to eliminate the interdigited electrode capacitance and parasitic capacitances. Prior to testing the mechanical behavior of the strain sensors, an estimation of the sensor capacitance values was obtained by the electron transport analysis method which is based on the extraction of the charging energy using the resistance data as a function of temperature (see eqn (7) ESI†). A capacitance value of 0.78 pF was deduced from eqn (2) using the E_C value extracted by the electron transport measurements performed at rest (Fig. S4 ESI†). This was achieved by taking an average gold NP diameter 7 nm, an inter-particle distance l = 1.2 nm for dodecanethiol (C12) ligands, ε_r = 2.3 typical for dodecanethiol. These capacitance values are in close agreement with values determined by previously determined calculations. Moreover, despite the inherent difficulties in producing reproducible filling of the interdigitated electrodes by NP assembly over such a large area of 1 mm^2, the three kinds of NP-based capacitive strain sensors had an initial capacitance C roughly around 1 pF, which agrees well with the theoretical values. In comparison the capacitance of the interdigited electrodes was around 1.65 pF. The electromechanical measurements were carried out using the force applied by the uniaxial traction machine (Deben Tensile Stage 200N) which generates a constant strain in the flexible substrate. The analyzed strain readings were taken every 0.1% for characterization of the strain sensitivity (the associated strength applied to the gauge increased from 0 N to 70 N). Fig. 4a represents the results for a typical capacitance measurement of three sensors with nanoparticles of various sizes. A large decrease in the relative capacitance as a function of strain is observed. Moreover, the relative capacitance variation increases as the size of the nanoparticle increases, with a maximum relative variation of −5.2% for a strain of 1.5% for the sensor composed of 14 nm NPs, giving a GF_C of approximately 3.5. This behavior matches the theoretical predictions presented in the first section. On the contrary, the structure without nanoparticles only exhibits a very small decrease (≪1%, equivalent to a GF_C = 0.075) in the relative capacitance as a function of strain due to the variation relative distance between electrodes.

Fig. 4a further shows that, at such strains, the relative capacitance output signal of the sensors begins to show the logarithmic dependence noted in the model presented in the first section. Further insight can be gained by considering the error bars of the model. Such error bars can be calculated by recognizing that different conformations can occur from the C12 ligands protecting two particles. An initial calculation of the inter-nanoparticle edge-to-edge distance of gold nanoparticles surrounded by C12 ligand alkyl chains can be approximated by the ligand length. The small-angle X-ray scattering (SAXS) measurements performed on increasing number of carbons on the alkyl chain exhibit a linear relationship with

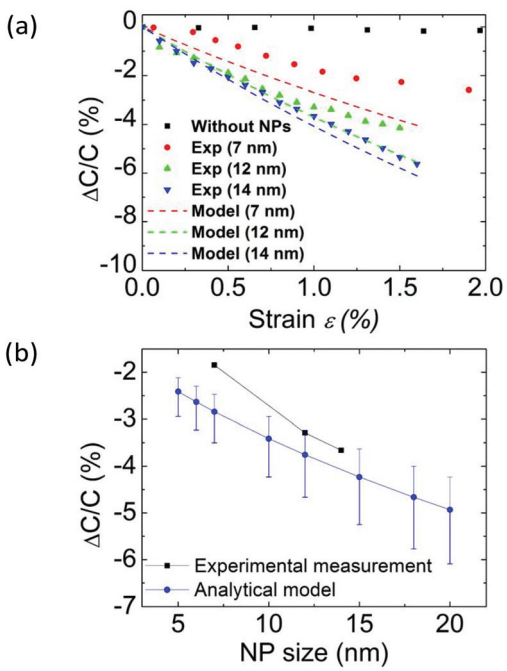

Fig. 4 (a) Experimental and analytical results of relative capacitance variation $\Delta C/C$ of NP-based capacitive strain sensors as a function of strain for nanoparticles of three different sizes and a structure without NPs (f = 10 kHz). (b) Evolution of the relative capacitance variation as a function of the nanoparticle size at 1% of strain (f = 10 kHz).

a slope of 0.11 nm per nanoparticles pair unit.[31] The dodecanethiol C12 ligand can thus be estimated *ca.* 1.2 nm. In addition, we performed auto-correlation processing performed with Gwyddion software using SEM images containing a high number of NPs to extract the inter-NP distance. We found that the inter-NP distance can vary between 1.2 nm ± 0.4 nm (Fig. S5 ESI†). We then used the 1.2 nm ± 0.4 nm internanoparticle distance to estimate the error bars which are indicated on the theoretical relative capacitance curve (Fig. 4b).

The slight difference between experimental and theoretical points can be explained by two phenomena which were not taken into account in our simple theoretical model. First, we already observed partial strain transfer from the substrate to the NP assembly in the case of resistive strain gauges.[43] Secondly, we cannot exclude a reorganization of the ligands under uniaxial strain which will imply a variation of the surrounding medium of the NPs and then a variation of the relative permittivity ε_r (see the ESI†). Our undergoing numerical simulations tend to show that decreasing the strain transmission coefficient (*e.g.* from 1 to 0.7) and increasing the relative permittivity (*e.g.* from 2.3 to 2.32) both lead to the decrease of the relative capacitance variation of the sensor under deformation. The difference between experimental and theoretical points will therefore be reduced significantly. Hence, despite a slight difference between theoretical and experiment values, Fig. 4b demonstrates that our simple model corresponds well with the experiments.

Moreover, the dynamical behavior of our NP-based capacitive strain sensor was evaluated by subjecting it to a series of bending cycles under tensile mode. For example, a sensor was stretched and released repeatedly from 0 to 1% strain, at a frequency of one cycle each 50 s. The time-dependence of its relative capacitance variation is reproducible, as is shown in Fig. 5, indicating a constant capacitive variation of the sensor with a small progressive downward drift of the capacitance at rest with each cycle, as compared to the initial capacitance C. This kind of drift was previously observed in resistive nanoparticle based sensors.[47] Most likely, the NP layer structure responds to strain with structural rearrangements, resulting in significant changes of the interparticle distances. This behavior was already depicted in comprehensive Small Angle X-ray Scattering and Grazing Incidence (SAXS/GISAXS) investigations on resistive nanoparticle strain sensors.[45] In addition, Lindsay *et al.*[46] reported results suggesting that the charge transport involves, to some extent, the alkyl chain of the linker molecules. As long as the nanoparticles remain interlinked, such an electron transport mechanism is less sensitive to changes in interparticle distances than a charge transport proceeding without molecular linkages between NPs.

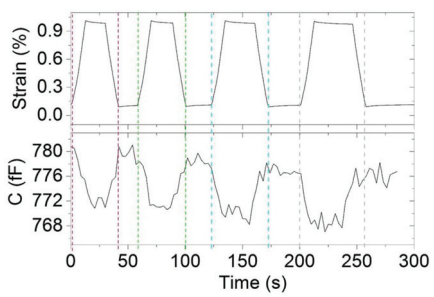

Fig. 5 Typical time-dependent response of a 7 nm NP-based capacitive strain sensor undergoing a series of strain cycles between 0 and 1% (f = 10 kHz).

IV.2 Influence of frequency on the sensor sensitivity

We already documented that gold NP assemblies can act as resistive strain gauges.[38] Our electron transport model analysis showed that the nanoparticle assemblies have both a resistive nature given by electrons passing through ligands towards nanoparticles as well as a capacitive nature given by nanoparticles as carrier reservoirs and ligands as insulators.[30] This suggests that the present capacitive gauges based on similar NP assemblies do not evince a pure ideal resistive or capacitive behavior and therefore must exhibit different features as a function of frequency measurement. This can be a primary advantage of NP-based capacitive sensors over NP-based resistive gauges since it makes it possible to adapt the overall sensor features (sensitivity, consumption...) by choosing the frequency. Indeed, as can be seen on the curves of the impedance module $|Z|$ and phase θ in Fig. 6a, the NP-based capacitive strain sensors behave differently as a function of the frequency. At low frequency they behave in a quasiresistive manner while it is necessary to go beyond 1 MHz to have pure capacitance.

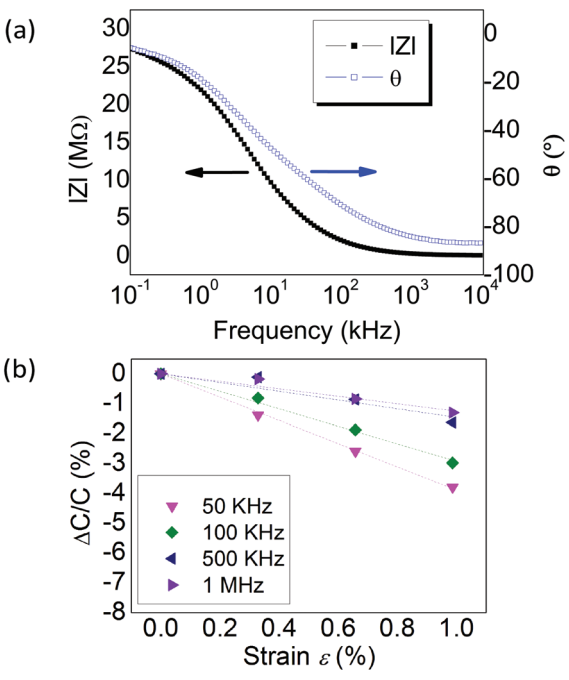

Fig. 6 (a) Typical module and phase of the equivalent impedance model for 7 nm NP-based capacitive strain sensor. (b) Evolution of its relative capacitance as a function of frequency measurements for frequencies ranging from 50 kHz to 1 MHz.

This frequency dependence is due to the several particular features of the strain sensors. At low frequency, the sensor capacitance is affected by the resistance of the NP assembly and the dispersion capacitance, which is frequency-dependent and associated with hole or electron emission from slowly responding deep impurity levels.[31] This explanation is corroborated by temperature-dependent capacitance and resistance measurements presented in Fig. 7. Indeed, frequency measurements as a function of temperature clearly show that the resistance decreases and the capacitance increases when the temperature increases. Moreover, the slope of the capacitance curves decreases when the temperature decreases suggesting that capacitance variations are smaller at low temperatures. This can be understood in terms of E_C and k_BT comparison. Indeed, at low temperatures, k_BT is much lower than E_C (~25 meV), making it difficult for electrons to pass from one NP to another. As a result, the capacitance value of the NP-based capacitive strain sensors are more effective than at high temperatures where the electrons can be swept away by thermal energy. At the same time, the electrons have difficulty passing from one reservoir to another; this implies an increase in resistance when the temperature decreases as shown in Fig. 7a. Hence, the capacitive behavior will be more pronounced at low temperatures explaining why the capacitance is dependent on the frequency at high temperatures (Fig. 7b).

As the frequency is increased, the frequency-independent capacitance begins to overcome the resistive behavior of the sensors, as suggested by the phase signal which approaches −90 °C (Fig. 6a). As clearly seen in Fig. 6a, the pronounced capacitance behavior can be estimated to be over 500 kHz for the 7 nm NP-based sensors. At the same time, Fig. 6b shows that the relative capacitance of the sensors is dependent on the frequency. But as can be seen clearly, this frequency dependence disappears when the sensor capacitance enters the "pronounced" capacitance region previously mentioned (*i.e.* beyond 500 kHz). However, Fig. 6b reveals that the GF_C is frequency dependent and increases for decreasing frequencies.

Hence, the overall electrical behavior confirms that these NP-based capacitive strain sensors must be modeled by a resistance and capacitance which are in parallel, as indicated by Fig. S1 ESI.† The use of these strain sensors will therefore require a compromise between a pure capacitive domain (constant relative capacitance with frequency) and an increased sensitivity for a mixed capacitive–resistance domain. Indeed, it is worth noting that a greater gauge factor is obtained with our previously produced resistive strain gauges under the same conditions.[44]

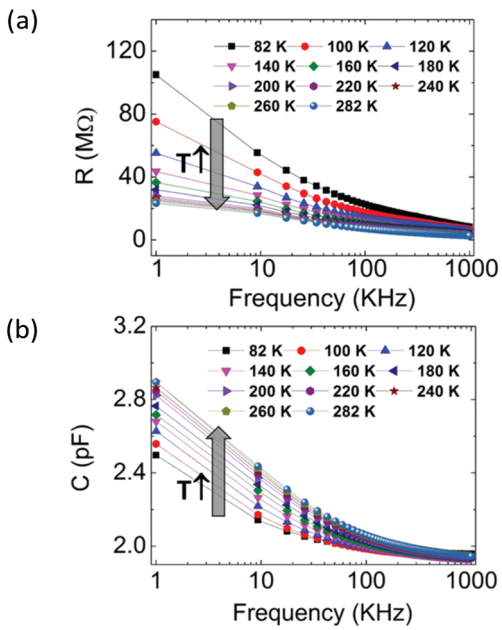

Fig. 7 Typical resistance–frequency (a) and capacitance–frequency (b) characteristics of 7 nm NP-based capacitive strain sensor as a function of temperature.

V Low-cost capacitive strain measurements

In order to realize the large-scale wireless deployment of such sensors, the first step is to build low-cost equipment and verify that it is sensitive to such low capacitance values. Several options exist to associate these capacitive transducers with a conditioning electronic circuit capable of exploiting capacitance variations. It is then possible to use a heterodyne circuit, insofar as we are able to produce two identical sensors. It would also be possible to integrate these transducers in an oscillating circuit whose frequency would follow its capacitance variations. Moreover, the transducers could also be integrated in a simple push–pull circuit. However, before implementing any of these solutions, we tested a very simple and low-cost assembly based on a Teensy development board using a 32 bit ARM processor.[49]

This microcontroller is interesting because it has a so-called "touch sensing input" (TSI) module providing capacitive touch sensing detection with high sensitivity and enhanced robustness.

The electrode capacitance measurement unit (Fig. 8a) senses the capacitance of a TSI pin and outputs a 16-bit result. This module is based on dual oscillator architecture. One oscillator is connected to the external electrode array and oscillates according to the electrode capacitance, while the other according to an internal reference capacitor. The pin capacitance measurement is provided by the counted number of periods of the reference oscillator during a predefined number of electrode oscillations. The electrode oscillator charges and discharges the pin capacitance with a programmable current source to accommodate several different sizes of electrode capacitances. The electrode oscillator frequency, before being compared to that of the reference oscillator, goes through a prescaler and module counter to decrease its frequency and consecutively increase the measurement resolution and noise

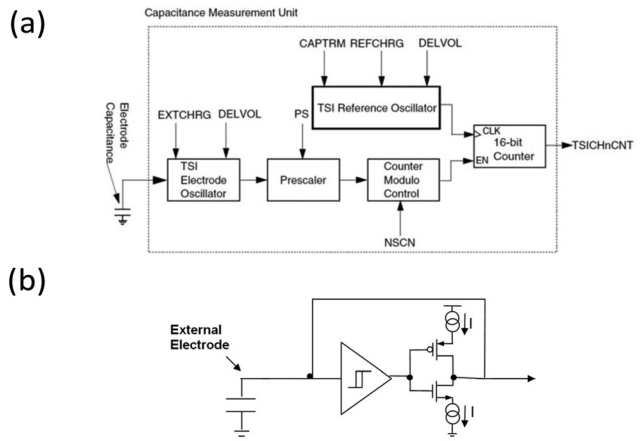

Fig. 8 (a) TSI capacitance measurement unit block diagram, (b) TSI electrode oscillator circuit.

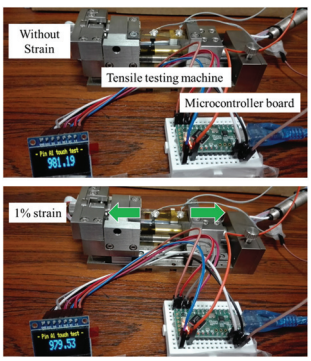

Fig. 9 Simple and low-cost measurement method for detecting the capacitance variations of the NP-based strain sensors at low strain based on a microcontroller connected to an OLED screen: (top) manipulation image before strain (bottom) manipulation image after strain.

robustness. Fig. 8 presents the simplified block diagram of how the electrode capacitance is measured.

The input electrode oscillator (Fig. 8b) is based on a configurable constant current source used to charge and discharge the external electrode capacitance. A buffer hysteresis defines the oscillator delta voltage which defines the margins of high and low voltage which are the reference input of the comparator at various times. As shown in Fig. 9 when a strain of 1% was applied to a 12 nm NP-based capacitive strain sensor the values displayed on the screen decreased 2–3 units while the measurement errors were in the range of 0.005 unit. The difference in these values can be directly related to the variation in capacitance which is in the order of hundred fF.

This simple low-cost circuit can detect capacitance variations generated by our capacitive sensors at such a low strain.

This proves that we have built a low-cost equipment that paves the way for the development of a whole wireless application set-up.

VI Conclusions

We describe the design, fabrication and testing of new capacitive strain sensors based on gold colloidal nanoparticles deposited in between interdigitated electrodes created on a flexible substrate. The design of these strain sensors was first optimized thanks to an analytical model in order to achieve maximum capacitance values and strain sensitivity. The sensors were then fabricated with the simple and low-cost technique of convective assembly allowing the deposition of a close-packed assembly of gold nanoparticles in between interdigitated electrodes over 1 mm^2. Electro-mechanical experiments revealed that such sensors exhibit measurable capacitances (>∼1 pF) and present sensitivities around five times higher than those found in the literature for other capacitive strain sensors. These experimental results are certainly in good agreement with our analytical model. A series of bending cycles under tensile mode confirmed the robustness and reliability of the fabricated sensors. We demonstrated that the existence of two domains (pure capacitive domain and mix capacitive–resistance domain) as a function of the frequency measurement makes it possible to adapt the sensitivity and the overall consumption of these capacitive sensors. Finally, measurements of the capacitance variations of the NP-based capacitive strain sensors at low strain by a simple and low-cost circuit based on a microcontroller demonstrated that these sensors are ready for large-scale deployment, paving the way for the development of a whole wireless application setup.

Conflicts of interest

There are no conflicts to declare.

Acknowledgements

This work was supported by “Initiatives d’excellence IDEX UNITI” in the framework of its program “Actions Thématiques Stratégiques” AAP 2015 (Project “WE CAN”). The authors thank Y. Leroy and A. S. Cordan for fruitful discussions on the capacitance modeling. We are very grateful to Paula Wisotzki, Ph.D. Professor at Loyola University of Chicago and Thomas F. Rowlands, Ph.D for proofreading the article.

References

1 R. K. Yedavalli and R. K. Belapurkar, Application of wireless sensor networks to aircraft control and health management systems, *J. Control Theory Appl.*, 2011, **9**(1), 28–33.

2 X. Riedl, C. Bolzmacher, R. Wagner, K. Bauer, N. Schwesinger, A novel PDMS based capacitive pressure sensor, Sensors, 2010 IEEE, pp. 2255–2258.

3 P. Peng and R. Rajamani, Flexible microtactile sensor for normal and shear elasticity measurements, *IEEE Trans. Ind. Electron.*, 2012, **59**(12), 4907–4913.

4 J. Aebersold, *et al.*, Design, modeling, fabrication and testing of a MEMS capacitive bending strain sensor, *J. Phys.: Conf. Ser.*, 2006, **34**, 124.

5 K. I. Arshak, D. McDonagh and M. A. Durcan, Development of new capacitive strain sensors based on thick film polymer and cermet technologies, *Sens. Actuators, A*, 2000, **79**(2), 102–114.

6 R. Matsuzaki and A. Todoroki, Wireless flexible capacitive sensor based on ultra-flexible epoxy resin for strain measurement of automobile tires, *Sens. Actuators, A*, 2007, **140**(1), 32–42.

7 R. Zeiser, T. Fellner and J. Wilde, *Development and testing of capacitive strain gauges*, Univ. Freibg., Web Rep., 2010.

8 D. J. Lichtenwalner, A. E. Hydrick and A. I. Kingon, Flexible thin film temperature and strain sensor array utilizing a novel sensing concept, *Sens. Actuators, A*, 2007, **135**(2), 593–597.

9 M. C. LeMieux and Z. Bao, Flexible electronics: stretching our imagination, *Nat. Nanotechnol.*, 2008, **3**(10), 585–586.

10 W. C. W. Chan, B. Y. S. Kim and J. T. Rutka, Current concepts: nanomedicine, *N. Engl. J. Med.*, 2010, **363**, 2434–2443.

11 F. Ilievski, A. D. Mazzeo, R. F. Shepherd, X. Chen and G. M. Whitesides, *Angew. Chem., Int. Ed.*, 2011, **50**, 1890–1895.

12 R. Zeiser, T. Fellner and J. Wilde, Capacitive strain gauges on flexible polymer substrates for wireless, intelligent systems, *J. Sens. Sens. Syst.*, 2014, **3**(1), 77.

13 V. Tsouti, V. Mitrakos, P. Broutas and S. Chatzandroulis, Modeling and Development of a Flexible Carbon Black Based Capacitive Strain Sensor, *Sensors*, 2014, **10466**(R1), 1.

14 O. Kasyutich, R. D. Desautels, B. W. Southern and J. Van Lierop, Novel aspects of magnetic interactions in a macroscopic 3D nanoparticle-based crystal, *Phys. Rev. Lett.*, 2010, **104**(12), 127205.

15 S. Li, H. Liu, L. Liu, L. Tian and N. He, A novel automated assay with dual-color hybridization for single-nucleotide polymorphisms genotyping on gold magnetic nanoparticle array, *Anal. Biochem.*, 2010, **405**(1), 141–143.

16 N. Krasteva, *et al.*, Self-assembled gold nanoparticle/dendrimer composite films for vapor sensing applications, *Nano Lett.*, 2002, **2**(5), 551–555.

17 H. Nakanishi, *et al.*, Photoconductance and inverse photoconductance in films of functionalized metal nanoparticles, *Nature*, 2009, **460**(7253), 371.

18 C. Farcau, *et al.*, Monolayered wires of gold colloidal nanoparticles for high-sensitivity strain sensing, *J. Phys. Chem. C*, 2011, **115**(30), 14494–14499.

19 T. Vossmeyer, C. Stolte, M. Ijeh, A. Kornowski and H. Weller, Networked Gold-Nanoparticle Coatings on Polyethylene: Charge Transport and Strain Sensitivity, *Adv. Funct. Mater.*, 2008, **18**(11), 1611–1616.

20 J. Herrmann, *et al.*, Nanoparticle films as sensitive strain gauges, *Appl. Phys. Lett.*, 2007, **91**(18), 183105.

21 M. A. Lim, Y. W. Lee, S. W. Han and I. Park, Novel fabrication method of diverse one-dimensional Pt/ZnO hybrid nanostructures and its sensor application, *Nanotechnology*, 2010, **22**(3), 035601.

22 P. Murugaraj, D. Mainwaring, N. A. Khelil, J. L. Peng, R. Siegele and P. Sawant, The improved electromechanical sensitivity of polymer thin films containing carbon clusters produced in situ by irradiation with metal ions, *Carbon*, 2010, **48**(15), 4230–4237.

23 R. Parthasarathy, X.-M. Lin and H. M. Jaeger, Electronic transport in metal nanocrystal arrays: The effect of structural disorder on scaling behavior, *Phys. Rev. Lett.*, 2001, **87**(18), 186807.

24 W. P. Wuelfing, S. J. Green, J. J. Pietron, D. E. Cliffel and R. W. Murray, Electronic conductivity of solid-state, mixed-valent, monolayer-protected Au clusters, *J. Am. Chem. Soc.*, 2000, **122**(46), 11465–11472.

25 Y. Zhang, O. Dai, M. Levy and M. P. Sarachik, Probind the Coulomb Gap in Insulating n-Type CdSe, *Phys. Rev. Lett.*, 1990, **64**(22), 2687.

26 K.-H. Müller, J. Herrmann, B. Raguse, G. Baxter and T. Reda, *Phys. Rev. B: Condens. Matter Mater. Phys.*, 2002, **66**, 075417.

27 K.-H. Müller, G. Wei, B. Raguse and J. Myers, *Phys. Rev. B: Condens. Matter Mater. Phys.*, 2003, **68**, 155407.

28 J. Liao, Y. Zhou, C. Huang, Y. Wang and L. Peng, Fabrication, transfer, and transport properties of monolayered freestanding nanoparticle sheets, *Small*, 2011, **7**(5), 583–587.

29 V. Aleksandrovic, *et al.*, Preparation and electrical properties of Cobalt- Platinum nanoparticle monolayers deposited by the Langmuir- Blodgett technique, *ACS Nano*, 2008, **2**(6), 1123–1130.

30 J. Grisolia, N. Decorde, M. Gauvin, N. M. Sangeetha, B. Viallet and L. Ressier, Electron transport within transparent assemblies of tin-doped indium oxide colloidal nanocrystals, *Nanotechnology*, 2015, **26**(33), 335702.

31 T. B. Tran, I. S. Beloborodov, J. Hu, X. M. Lin, T. F. Rosenbaum and H. M. Jaeger, Sequential tunneling and inelastic cotunneling in nanoparticle arrays, *Phys. Rev. B: Condens. Matter Mater. Phys.*, 2008, **78**(7), 075437.

32 B. Abeles, P. Sheng, M. D. Coutts and Y. Arie, Structural and electrical properties of granular metal films, *Adv. Phys.*, 1975, **24**(3), 407–461.

33 P. Beecher, A. J. Quinn, E. V. Shevchenko, H. Weller and G. Redmond, Insulator-to-metal transition in nanocrystal assemblies driven by in situ mild thermal annealing, *Nano Lett.*, 2004, **4**(7), 1289–1293.

34 A. S. Cordan, Occurrence of giant current fluctuations in 2D tunnel junction arrays, *Solid-State Electron.*, 2004, **48**(3), 445–452.

35 Y. Suganuma and A.-A. Dhirani, Gating of enhanced electron-charging thresholds in self-assembled nanoparticle films, *J. Phys. Chem. B*, 2005, **109**(32), 15391–15396.

36 A. J. Quinn, *et al.*, Manipulating the charging energy of nanocrystal arrays, *Small*, 2005, **1**(6), 613–618.
37 C.-Y. Lee, G.-W. Wu and W. Hsieh, Fabrication of micro sensors on a flexible substrate, *Sens. Actuators, A Phys.*, 2008, **147**(1), 173–176.
38 H. Moreira, *et al.*, Electron transport in gold colloidal nanoparticle-based strain gauges, *Nanotechnology*, 2013, **24**(9), 095701.
39 N. Zheng, J. Fan and G. D. Stucky, One-step one-phase synthesis of monodisperse noble-metallic nanoparticles and their colloidal crystals, *J. Am. Chem. Soc.*, 2006, **128**(20), 6550–6551.
40 P. Braunstein, H. Lehner, D. Matt, K. Burgess and M. J. Ohlmeyer, A Platinum-Gold Cluster: Chloro-1κCl-Bis (Triethylphosphine-1κP) Bis (Triphenyl-Phosphine)-2κP, 3κP-Triangulo-Digold-Platinum (1+) Trifluoromethanesulfonate, *Inorg. Synth.*, 2007, **27**, 218–221.
41 H. Hiramatsu and F. E. Osterloh, A simple large-scale synthesis of nearly monodisperse gold and silver nanoparticles with adjustable sizes and with exchangeable surfactants, *Chem. Mater.*, 2004, **16**(13), 2509–2511.
42 C. Stanglmair and C. Pacholski, *Eur. J. Inorg. Chem.*, 2014, 3633–3637.
43 N. Decorde, N. M. Sangeetha, B. Viallet, G. Viau, J. Grisolia, A. Coati, A. Vlad, Y. Garreau and L. Ressier, *Nanoscale*, 2014, **6**, 15107–15116, DOI: 10.1039/C4NR04129A.
44 C. Farcau, *et al.*, High-sensitivity strain gauge based on a single wire of gold nanoparticles fabricated by stop-and-go convective self-assembly, *ACS Nano*, 2011, **5**(9), 7137–7143.
45 N. M. Sangeetha, N. Decorde, B. Viallet, G. Viau and L. Ressier, *J. Phys. Chem. C*, 2013, **117**(4), 1935–1940.
46 X. D. Cui, A. Primak, X. Zarate, J. Tomfohr, O. F. Sankey, A. L. Moore, T. A. Moore, D. Gust, L. A. Nagahara and S. M. Lindsay, *J. Phys. Chem. B*, 2002, **106**, 8609.
47 M. Gauvin, *et al.*, Electro-mechanical sensing in freestanding monolayered gold nanoparticle membranes, *Nanoscale*, 2016, **8**(22), 11363–11370.
48 M. Gauvin, *et al.*, Plasmonic photo-current in freestanding monolayered gold nanoparticle membranes, *Nanoscale*, 2016, **8**(36), 16162–16167.
49 K20 Sub-Family Reference Manual, Rev. 1.1, Dec 2012 - Google Search. [Online]. Available: https://www.google.fr/search?q=K20+Sub-Family+Reference+Manual%2C+Rev.+1.1%2C+Dec+2012&rlz=1C1CHBF_frFR728FR728&oq=K20+Sub-Family+Reference+Manual%2C+Rev.+1.1%2C+Dec+2012&aqs=chrome..69i57.803j0j7&sourceid=chrome&ie=UTF-8 [accessed: 23-Nov-2017].